

Nitric Oxide Reacts Very Fast with Hydrogen Sulfide, Alcohols, and Thiols to Produce HNO: Revised Rate Constants

Nicolas I. Neuman,[†] Mateus F. Venâncio,[†] Willian R. Rocha, Damian E. Bikiel, Sebastián A. Suárez,^{*} and Fabio Doctorovich^{*}



Cite This: <https://doi.org/10.1021/acs.inorgchem.1c01061>



Read Online

ACCESS |



Metrics & More

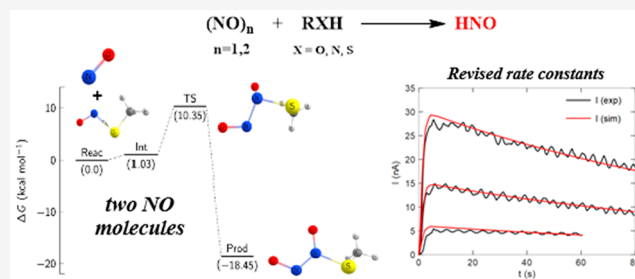


Article Recommendations



Supporting Information

ABSTRACT: The chemical reactivity of NO and its role in several biological processes seem well established. Despite this, the chemical reduction of $\bullet\text{NO}$ toward HNO has been historically discarded, mainly because of the negative reduction potential of NO. However, this value and its implications are nowadays under revision. The last reported redox potential, $E^\circ(\text{NO}, \text{H}^+/\text{HNO})$, at micromolar and picomolar concentrations of $\bullet\text{NO}$ and HNO, respectively, is between -0.3 and 0 V at pH 7.4. This potential implies that the one-electron-reduction process for NO is feasible under biological conditions and could be promoted by well-known biological reductants with reduction potentials of around -0.3 to -0.5 V. Moreover, the biologically compatible chemical reduction of $\bullet\text{NO}$ (nonenzymatic), like direct routes to HNO by alkylamines, aromatic and pseudoaromatic alcohols, thiols, and hydrogen sulfide, has been extensively explored by our group during the past decade. The aim of this work is to use a kinetic modeling approach to analyze electrochemical HNO measurements and to report for the first-time direct reaction rate constants between $\bullet\text{NO}$ and moderate reducing agents, producing HNO. These values are between 5 and 30 times higher than the previously reported k_{eff} values. On the other hand, we also showed that reaction through successive attack by two NO molecules to biologically compatible compounds could produce HNO. After over 3 decades of intense research, the $\bullet\text{NO}$ chemistry is still there, ready to be discovered.



1. INTRODUCTION

Since the discovery of the physiological role of $\bullet\text{NO}$ in the 1980s, the chemical and biochemical reactivity of this small molecule was studied in detail over the following decades, and it still continues to be reviewed.^{1–9} Azanone (HNO/NO^-) or nitroxyl is the one-electron-reduction product of $\bullet\text{NO}$, and its reactivity and biological relevance are currently under intense debate.^{10–13} HNO dimerizes very fast ($k_{\text{dim}} = 8 \times 10^6 \text{ M}^{-1} \text{ s}^{-1}$),¹⁴ which limits its concentration and lifetime in solution. Moreover, HNO reacts fast with its sibling $\bullet\text{NO}$ ($k_{\text{NO}, \text{HNO}} = 5.6 \times 10^6 \text{ M}^{-1} \text{ s}^{-1}$)¹⁵ and at a moderate rate ($k_{\text{HNO}, \text{O}_2} = 3 \times 10^3 \text{ M}^{-1} \text{ s}^{-1}$) with oxygen.^{14,16,17} Interestingly, despite the overlapping reactivity of both compounds in biological media^{18,19} with oxygen, thiols, ascorbic acid, transition metals,^{20,21} and hemoproteins,^{22–25} the biochemical pathways turn out to be very different.^{26,27}

The proposed reduction potential for the $\bullet\text{NO}/^3\text{NO}^-$ couple is -0.8 V.¹² This was obtained by Bartberger et al. in 2002 with a combination of experimental and computational methods and has been the most reliable value in the literature since then.²⁸ Our calculation of this reduction potential through TPSSh-D3(BJ)/def2-QZVP/COSMO(SMD) yielded a reduction potential of -0.81 V, which is in excellent agreement with the accepted value.²⁹ Experimental irreversible

reduction of $\bullet\text{NO}$ at a Hg electrode was shown to occur at a potential of -1.0 V versus saturated calomel electrode, and N_2O was the only detected product.^{30,31}

However, at physiological pH, HNO is the main species with an estimated $E^\circ(\bullet\text{NO}, \text{H}^+/\text{HNO}) \approx -0.11$ V, which becomes -0.55 V at pH 7.¹² In contrast to the well-accepted value for the NO/NO^- reduction potential, the $\bullet\text{NO}/\text{HNO}$ reduction potential is not completely established. Shafirovich and Lyman derived in 2002 the value of -0.55 V at pH 7 by using values for $\Delta_f G^\circ(\bullet\text{NO}_{\text{aq}}) = 102 \text{ kJ mol}^{-1}$ and the gas-phase enthalpy of formation for ^1HNO of 107 kJ mol^{-1} (as recommended by W. R. Andersson),³² as well as the tabulated entropy $S^\circ(\text{HNO}_{\text{gas}}) = 220.7 \text{ J mol}^{-1} \text{ K}^{-1}$ and approximations for the free energy of formation of HNO in aqueous solution, $\Delta_f G^\circ(^1\text{HNO}_{\text{aq}})$, which were calculated by estimating the HNO hydration energy as similar to the hydration energy of HCN and H_2CO . This value has been revised in 2017 by Rocha et al.²⁹ The authors

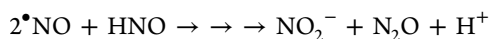
Special Issue: Renaissance in NO Chemistry

Received: April 6, 2021

computed the reduction potential at pH 7 in aqueous solution using quantum-mechanical calculations and Monte Carlo statistical mechanical simulations. It was derived as an efficient protocol to obtain the solvation free energy of HNO using three different computational approaches. A combination of linear response theory and continuum solvation approaches (COSMO/SMD) for more than a hundred uncorrelated structures obtained from Monte Carlo simulations was used to obtain $-4.62 \text{ kcal mol}^{-1}$ as the solvation free energy of HNO, which is at least 2 times greater than the value of -5 kJ mol^{-1} previously estimated by Shafirovich and Lyman in 2002, on the basis of chemically related compounds. Considering the 2017 protocol, it seems reasonable to take for the $\bullet\text{NO}/\text{HNO}$ reduction potential in aqueous solution, the value obtained by Rocha and co-workers, $E^\circ = -0.16 \text{ V}$ at pH 7,²⁹ showing that it is a viable process under physiological conditions.

Liochev and Fridovich had discussed the possibility of the production of NO/HNO within living cells.¹⁷ The equilibrium redox potential for $\bullet\text{NO}/\text{HNO}$ in the cell can be much less negative because the $[\bullet\text{NO}]/[\text{HNO}]$ ratio can be high, and according to the Nernst equation, its logarithm influences the actual redox potential. In this context, using the $E^\circ(\text{NO}, \text{H}^+/\text{HNO}) \approx -0.11 \text{ V}$, the calculated redox potential E' at micromolar and picomolar concentrations of NO and HNO, respectively, is between -0.30 and 0 V at pH 7.4. These redox values are compatible with the observed reactions of NO with alcohols, thiols, and HS^- , as will be described in more detail below.

Pryor, De Master, and co-workers found that anaerobic aqueous solutions of thiols and thiol-containing proteins exposed to NO result in quantitative formation of the corresponding disulfides (RSSR) or sulfenic acids $\text{RS}-\text{OH}$.^{33,34} These reactions, which took place in minutes, were shown to produce N_2O . The authors disregarded HNO as a reaction intermediate, possibly because of the lack of selective detection methods for HNO, with all being indirect at the moment (1980s and 1990s). In this context, during the past decade, the biologically compatible chemical reduction of $\bullet\text{NO}$ (nonenzymatic) as direct routes to HNO was explored by our group.^{35–40} The reduction of $\bullet\text{NO}$ to HNO has to be necessarily coupled to other reactions that produce compounds such as N_2O , driving the reaction forward and overcoming an unfavorable thermodynamic barrier. This chemical reductive route recently received key support, showing that $\bullet\text{NO}$ can be converted to HNO by the aforementioned thiols,³⁷ but also by hydrogen sulfide,^{35,40,41} aromatic and pseudoaromatic alcohols (i.e., ascorbic acid, tyrosine, and salicylic acid),^{36,39} and alkylamines.³⁸ In all cases, the final concentrations of nitrite in solution and the amount of N_2O in the reaction chamber headspace were determined. Both were produced in approximately a 1:1 ratio, as was expected to occur due to the reaction between HNO and $\bullet\text{NO}$.



In previous work, we reported the effective rate constants k_{eff} for the reactions of NO with the mentioned reductants in anoxic conditions.⁴² These estimated values are a result of the combined generation and consumption pathways. Because the decay of HNO is extremely fast (see above), these values are underestimations and imply that the “real” rate constants have to be larger. A more detailed discussion of the relationship between the “effective” and “real” rate constants is given in Section 2.2 and the Supporting Information (SI).

In this work, first of all, we developed a kinetic modeling approach to analyze electrochemical HNO measurements, in order to determine, for the first time, the direct $k_{\text{RXH,NO}}$ rate constant for the reaction between $\bullet\text{NO}$ and ascorbic acid, cysteine, and H_2S , as a proof of concept. These values are up to 6 times higher than the previously reported k_{eff} values. On the other hand, we also showed that the reaction of the successive attack by two $\bullet\text{NO}$ molecules to biologically compatible compounds could produce HNO.

2. MATERIALS AND METHODS

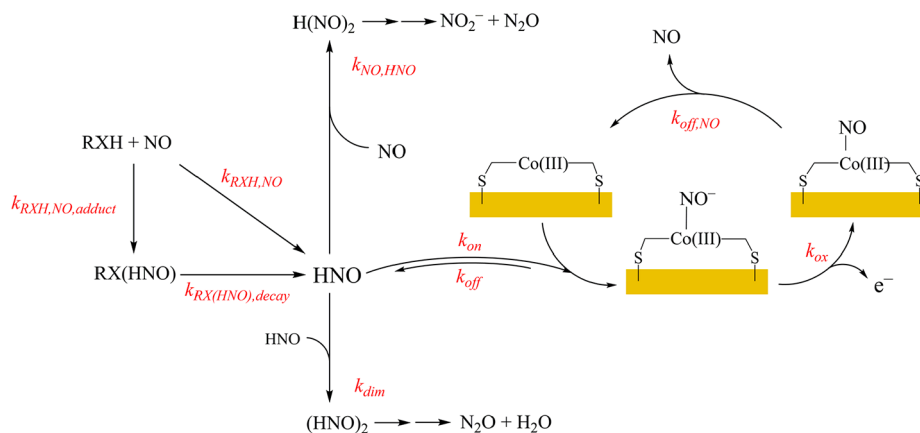
2.1. Experimental Procedures. Reagents. Cobalt(II) 5,10,15,20-tetrakis[3-(*p*-acetylthiopropoxy)phenyl]porphyrin was purchased from Frontiers Scientific. All other reagents were purchased from Sigma-Aldrich and used as received. NO was generated anaerobically by the dropwise addition of degassed water to a mixture of 4 g of NaNO_2 , 8.5 g of FeSO_4 , and 8.5 g of NaBr. The produced NO was passed through a NaOH solution to remove higher oxides and bubbled into degassed water in order to get a saturated solution of NO ($[\text{NO}] = 2 \text{ mM}$). This solution was kept under a strictly anaerobic NO atmosphere and injected into the electrochemical cell using a gastight syringe. The solutions of H_2S were prepared by bubbling with $\text{H}_2\text{S}(\text{g})$ and dissolving Na_2S . The reaction rate obtained was similar using both methods, so it does not seem to be influenced by the typical impurities present in NaHS (it is enriched with polysulfides).

Amperometric measurements of the HNO concentration were carried out as previously described.^{43–45} A three-electrode system consisting of a Pt counter electrode, a Ag/AgCl reference electrode, and a working electrode consisting of Au modified with a monolayer of cobalt porphyrin with 1-decanethiol which was covalently attached. The method was demonstrated to be specific for HNO, showing no interference or spurious signal due to the presence of NO, O_2 , NO_2^- , and other RNOS. Signal recording was performed with a TEQ 03 potentiostat. For each case, we also confirmed that the maximum employed concentrations of NO and all organic reductants produced negligible signals by themselves.

2.2. Kinetic Modeling of Reactions of $\bullet\text{NO}$ with Reductants to Produce HNO. In previous work, we have utilized an HNO-specific electrode for sensing HNO concentrations as functions of time and applied it to the analysis of several reactions that were shown to produce HNO, as well as reactions of HNO with different chemical and biological targets.^{44–46} In order to retrieve detailed kinetic information related to HNO generation and consumption, a fairly complicated kinetic model is necessary, and we have developed and used this model on occasions.^{44,46} In many other cases, we used, for simplicity, the electric current traces obtained with the electrode in a semiquantitative way. The electric current traces for HNO sensing usually show a relatively fast increase, which peaks and then decays with different rates. In a full kinetic analysis, the slope of the initial increase, the peak current, and the shape and rate of the decrease of the current after the peak all contain relevant information. In the simplified approach, only the peak current and position in time are used. The peak current is transformed to a maximum concentration of HNO, $[\text{HNO}]_{\text{max}}$ by calibration with a standard curve derived from the addition of Angeli's salt (AS) to the cell, which has a known decomposition constant. Then an effective rate velocity for each experiment is derived as

$$v_{\text{eff}} \approx \frac{\Delta[\text{HNO}]_{\text{max}}}{\Delta t_{\text{max}}}$$

The order of the reaction is also derived from a plot of v_{eff} as a function of the reactant concentrations and a rate law is proposed, from which an “effective” rate constant k_{eff} can be derived. This is an empirical methodology that allows a comparison of several related reactions and allows one to obtain kinetic information from an otherwise very complicated reaction system.

Scheme 1. General Mechanism for HNO Generation from the Reaction of $\bullet\text{NO}$ with a Reducing RXH Molecule and Electrocatalytic Oxidation by the HNO-Specific Electrode


However, in certain situations, it is necessary, in order to gain more insight, to utilize a more complete kinetic model including the interaction of HNO with the electrode and several of the known reactions of HNO with other species. Although this model provides more information than the simplified “effective” rate model, it still requires many assumptions and simplifications. The numerical relationship between the “effective” and model-derived constants depends on which pathways for HNO generation and consumption are included in the model. Two possible cases are discussed further in the SI.

Determination of the kinetic rate constants for HNO generation and consumption using our previously reported HNO-specific electrode^{36,37,44,46} involves simulations of current traces derived from the binding of HNO to an electrode-anchored cobalt(III) porphyrin, followed by its electrocatalytic oxidation to $\bullet\text{NO}$ and subsequent release. The simulations require the solution of a large set of coupled differential equations that include the catalytic cycle occurring at the surface of the electrode, as well as different HNO generation and consumption routes that occur in the bulk. The general mechanistic model is shown in Scheme 1, where the rate constants involved in the model are written in red.

For example, while the formation of a semistable RX(HNO) adduct (we do not specify the charge or spin state of this adduct) may be modeled by a simple bimolecular reaction step, with a single constant $k_{\text{RXH,NO,adduct}}$, its subsequent decay to release HNO may occur through several different pathways. This is most likely the case in the reaction of $\bullet\text{NO}$ with thiols, which will be discussed in the following sections. Therefore, the rate constant $k_{\text{RX(HNO),decay}}$ must be seen as a phenomenological unimolecular reaction rate, which does not imply a particular mechanism. The necessity of inclusion of the adduct in the kinetic modeling will become clear below.

The set of differential equations that describe the reactions occurring at the surface of the electrode are shown below. The suffix “elec” (short for electrochemical) in the differential equation for HNO indicates that these terms include only the reactions at the electrode surface. F is Faraday’s constant.

$$\frac{dI}{dt} = k_{\text{ox}}F \frac{d[\text{Co}^{\text{III}}\text{PNO}^-]}{dt} \quad (1)$$

$$\left(\frac{d[\text{HNO}]}{dt}\right)_{\text{elec}} = -k_{\text{on}}[\text{HNO}][\text{Co}^{\text{III}}\text{P}] + k_{\text{off}}[\text{Co}^{\text{III}}\text{PNO}^-][\text{H}^+] \quad (2)$$

$$\begin{aligned} \frac{d[\text{Co}^{\text{III}}\text{P}]}{dt} &= -k_{\text{on}}[\text{HNO}][\text{Co}^{\text{III}}\text{P}] + k_{\text{off}}[\text{Co}^{\text{III}}\text{PNO}^-][\text{H}^+] \\ &+ k_{\text{off,NO}}[\text{Co}^{\text{III}}\text{PNO}] \end{aligned} \quad (3)$$

$$\frac{d[\text{Co}^{\text{III}}\text{PNO}^-]}{dt} = k_{\text{on}}[\text{Co}^{\text{III}}\text{P}][\text{HNO}] - k_{\text{ox}}[\text{Co}^{\text{III}}\text{PNO}^-] \quad (4)$$

$$\frac{d[\text{Co}^{\text{III}}\text{PNO}]}{dt} = -k_{\text{off,NO}}[\text{Co}^{\text{III}}\text{PNO}] + k_{\text{ox}}[\text{Co}^{\text{III}}\text{PNO}^-] \quad (5)$$

Additionally, two decay routes for HNO are always included, which involve the reaction with $\bullet\text{NO}$ and HNO dimerization. The values for these rate constants were fixed from literature values ($k_{\text{HNO,NO}} = 5.8 \times 10^6 \text{ M}^{-1} \text{ s}^{-1}$ and $k_{\text{dim}} = 8 \times 10^6 \text{ M}^{-1} \text{ s}^{-1}$). The suffix “decay” refers to the contribution of these two reactions to the change in the HNO concentration.

$$\left(\frac{d[\text{HNO}]}{dt}\right)_{\text{decay}} = -k_{\text{NO,HNO}}[\text{HNO}][\text{NO}] - 2k_{\text{dim}}[\text{HNO}]^2 \quad (6)$$

$$\frac{d[\text{NO}]}{dt} = -k_{\text{NO,HNO}}[\text{HNO}][\text{NO}] \quad (7)$$

Finally, for each particular system, there will be specific HNO generation and decay pathways that will generate changes in the HNO and $\bullet\text{NO}$ concentrations in the bulk solution. These terms are labeled by the suffix “generation”. The total change in the HNO concentration can be written by the addition of the elec, decay, and generation terms in the differential equations, and similar expressions can be written for the $\bullet\text{NO}$ concentration.

$$\begin{aligned} \left(\frac{d[\text{HNO}]}{dt}\right)_{\text{total}} &= \left(\frac{d[\text{HNO}]}{dt}\right)_{\text{elec}} + \left(\frac{d[\text{HNO}]}{dt}\right)_{\text{decay}} \\ &+ \left(\frac{d[\text{HNO}]}{dt}\right)_{\text{generation}} \end{aligned} \quad (8)$$

The sets of differential equations were numerically solved, and the current versus time traces were simulated, using the ordinary differential equation (ode) functions in the GNU Octave program.⁴⁷

We have previously validated the model by simulating the current profile when different concentrations of AS (with a known decay constant of $9.1 \times 10^{-4} \text{ s}^{-1}$)⁴⁸ were added to the electrochemical cell. The obtained kinetic parameters are shown in Table 1. These are the same ones previously reported by us,⁴⁶ and we assume that they remained unchanged for the experiments with ascorbic acid, cysteine, or hydrogen sulfide.

2.3. Computational Details. Reaction Mechanisms. All geometries involved in the reaction mechanisms proposed in this work were obtained at the TPSSH-D3(BJ)/def2-TZVPP level of theory.^{49–51} In order to account for the effects of the solvent environment, the conductor-like polarizable-continuum model (C-PCM)⁵² in association with the solvation model based on density (SMD)⁵³ was employed on geometry optimizations. In order to

Table 1. Reactions and Rate Constants for Generation and Decay of HNO, Together with the Electrochemical Model of the HNO-Specific Electrode^a

reaction	rate constants
Generation	
$\text{AS}(\text{N}_2\text{O}_3^{2-}) + \text{H}^+ \rightarrow \text{HNO} + \text{NO}_2^-$ (9)	$k_{\text{AS}} = 9.1 \times 10^{-4} \text{ s}^{-1}$
Decay	
$\text{HNO} + \bullet\text{NO} \rightarrow \text{N}_2\text{O}_2^{*-} + \text{H}^+$ (10)	$k_{\text{NO,HNO}} = 5.8 \times 10^6 \text{ M}^{-1} \text{ s}^{-1}$
$\text{HNO} + \text{HNO} \rightarrow \text{N}_2\text{O} + \text{H}_2\text{O}$ (11)	$k_{\text{dim}} = 8 \times 10^6 \text{ M}^{-1} \text{ s}^{-1}$
Electrochemical	
$\text{Co}^{\text{III}}(\text{Por}) + \text{HNO} \rightarrow \text{Co}^{\text{III}}(\text{Por})(\text{NO}^-) + \text{H}^+$ (12)	$k_{\text{on}} = 3.1 \times 10^4 \text{ M}^{-1} \text{ s}^{-1}$ $k_{\text{off}} = 0 \text{ s}^{-1}$
$\text{Co}^{\text{III}}(\text{Por})(\text{NO}^-) \rightarrow \text{Co}^{\text{III}}(\text{Por})(\text{NO}) + \text{e}^-$ (13)	$k_{\text{ox}} = 0.089 \text{ s}^{-1}$ ^b
$\text{Co}^{\text{III}}(\text{Por})(\text{NO}) \rightarrow \text{Co}^{\text{III}}(\text{Por}) + \bullet\text{NO}$ (14)	$k_{\text{off,NO}} = 0.11 \text{ s}^{-1}$

^aThe amount of cobalt(III) porphyrin chemisorbed on the electrode surface is included in the model through an empirical concentration of 10^{-9} M. ^bThe oxidation rate constant depends on the applied potential. On our initial optimization of the HNO-specific electrode, we found that a potential of 800 mV gave the best response and always work at this potential.

characterize the species involved on each mechanism as a local minimum (absence of imaginary frequencies) or a transition state (only one imaginary frequency on the reaction coordinate mode), vibrational frequencies were also calculated at the same level of theory.

All of these calculations were also performed using the ORCA 4.2.1 software.⁵⁴

3. RESULTS AND DISCUSSION

3.1. Kinetic Analysis of Electrochemical HNO Sensing Experiments. We performed simulations of the HNO-specific electrode current responses for the reactions of $\bullet\text{NO}$ with three organic reductants: ascorbic acid (AA stands for ascorbic acid, while AAH^- stands for an ascorbate anion, which is the form at pH 7.5), L-cysteine (CysH), and H_2S . The experimental and simulated current traces are shown in Figure 1. The concentrations of reactants are given in the legend to Figure 1; the peak current values for the different traces increase approximately linearly with the concentrations of the reagents. The concentrations used in the CysH experiments are 1 order

of magnitude lower than those in the AAH^- experiments, and the ones used in the H_2S experiments are almost 1 order of magnitude lower still; however, similar peak currents are obtained, which indicate that the reaction rates between $\bullet\text{NO}$ and RXH decrease in the order $\text{RXH} = \text{H}_2\text{S} \gg \text{CysH} \gg \text{AAH}^-$.

Initially, the only HNO source considered in the mechanistic model was the direct reaction $\bullet\text{NO} + \text{RXH} \rightarrow \text{HNO} + \text{RX}\bullet$, where the $\text{RX}\bullet$ radical could be the ascorbyl radical,³⁶ or it could be a thiyl radical $\text{RS}\bullet$. Although these radicals would react further and be eliminated from the solution (by reaction with $\bullet\text{NO}$, disproportion of ascorbyl into dehydroascorbic and ascorbic acid, or disulfide bond formation), the fate of the radicals was not explicitly included in the models. This followed from the need to reduce the number of independent reaction rates included in the models. A set of initial simulations of the experimental data in Figure 1 reproduced very well the first few seconds of each experiment (fast rise of the current), but inevitably the models predicted a decay of the current, which was much faster than the experimental one. The reason for this fast decay was the extremely large $k_{\text{NO,HNO}}$ and k_{dim} rate constants. To explain this observation, we proposed the formation of an adduct between RXH and $\bullet\text{NO}$, which could act as an HNO “reservoir”, releasing HNO more slowly or directly reacting with the electrode and donating NO^- to the cobalt(III) porphyrin. This adduct is in agreement with experimental observations: in the case of the ascorbic acid reaction with NO, we observed an intermediate of the formula $\text{AA}(\text{H})\text{NO}\bullet$ by cryo-MS³⁶ and in the case of thiols, an $[\text{RSNOH}]\bullet$ adduct has been proposed before (Suarez et al. 2017 and references cited therein).³⁷ The inclusion of adduct formation and decay rate constants in the models allowed us to reproduce quite well the “rise” and “decay” regions of the current traces. The rate constants derived from simulation of the current traces in Figure 1 are shown in Table 2, and additional kinetic constants are written in Table S1. The SI also contains an analysis of the sensitivity of the simulations to different values of the rate constants (Figures S2–S4 and the surrounding text). Table 2 also includes effective rate constants between RXH and $\bullet\text{NO}$, reported in earlier works. These effective rate constants reflect reactions that were written in a minimal or simplified form. In some of these reactions, very unstable products are generated (such as $\text{S}^{\bullet-}$ in eq 23) that make the reaction, as written, highly energetically unfavorable. The true mechanisms must involve

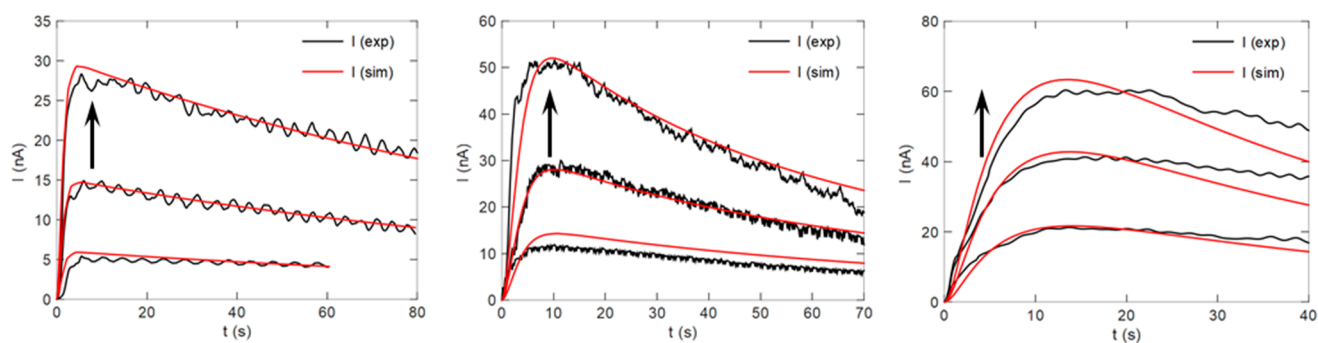
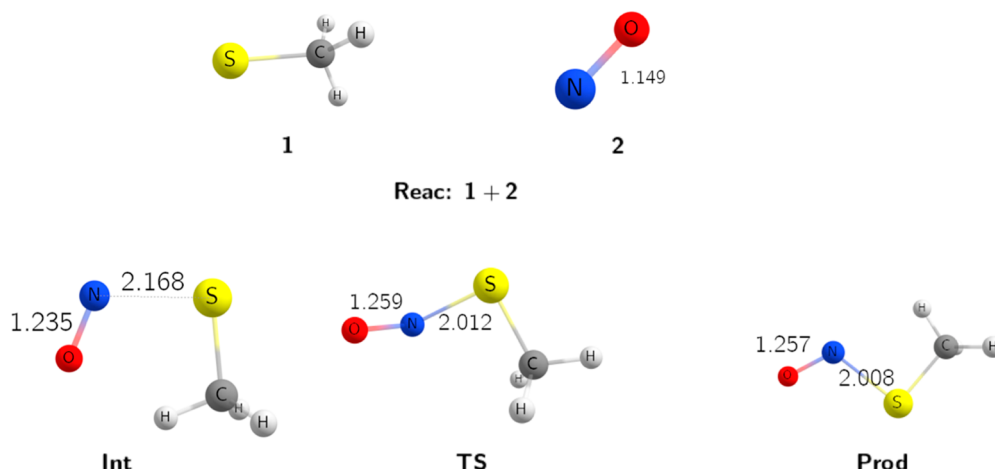


Figure 1. Experimental (black) and simulated (red) currents (I , nA) versus time (t , s) for reactions of AAH^- (0.4, 0.6, and 1 μM) with $\bullet\text{NO}$ (200 μM) (left), CysH (10 μM) with $\bullet\text{NO}$ (1, 2, and 3.8 μM) (middle), and H_2S (2 μM) with $\bullet\text{NO}$ (0.2, 0.4, and 0.6 μM) (right). The reactions were performed anaerobically at pH 7.4 (buffer phosphate) and with an applied potential of 800 mV. The arrows indicate the order of increasing concentration.

Table 2. Rate Constants for Adduct Formation and Decay or for Direct Reaction between RXH and NO, as Well as Effective Rate Constants Previously Reported^a

reaction	$k_{\text{RXH,NO,adduct}}$ or $k_{\text{RXH,NO,direct}}$	$k_{\text{RX(HNO),decay}}$	k_{eff}	ref
$\bullet\text{NO} + \text{AAH}^- \rightarrow \text{AAH(HNO)}^{\bullet-}$ (15)	28(4) $\text{M}^{-1} \text{s}^{-1}$			
$\text{AA(HNO)}^{\bullet-} \rightarrow \text{HNO} + \text{AAH}^{\bullet-}$ (16)		1.8(2) s^{-1}		
$\text{NO}^{\bullet} + \text{AAH}^- \rightarrow \text{HNO} + \text{AAH}^{\bullet-}$ (17)	43(15) $\text{M}^{-1} \text{s}^{-1}$ ^b		8(1) $\text{M}^{-1} \text{s}^{-1}$	36
$\bullet\text{NO} + \text{CysH} \rightarrow \text{Cys(HNO)}^{\bullet}$ (18)	180(20) $\text{M}^{-1} \text{s}^{-1}$			
$\text{Cys(HNO)}^{\bullet} \rightarrow \text{HNO} + \text{Cys}^{\bullet}$ (19)		0.5(1) s^{-1}		
$\bullet\text{NO} + \text{CysH} \rightarrow \text{HNO} + \text{Cys}^{\bullet}$ (20)	$8(1) \times 10^2 \text{M}^{-1} \text{s}^{-1}$		25(1) $\text{M}^{-1} \text{s}^{-1}$	37
$\bullet\text{NO} + \text{HS}^- \rightarrow \text{S(HNO)}^{\bullet-}$ (21)	$8(1) \times 10^3 \text{M}^{-1} \text{s}^{-1}$			
$\text{S(HNO)}^{\bullet-} \rightarrow \text{HNO} + \text{S}^{\bullet-}$ (22)		0.16(1) s^{-1}		
$\bullet\text{NO} + \text{HS}^- \rightarrow \text{HNO} + \text{S}^{\bullet-}$				
$\bullet\text{NO} + \text{HS}^- + \text{X/X}^{\bullet} \rightarrow \text{HNO} + \text{SY}^{\bullet-}/\text{SY}^-$ (23) ^c			$6(1) \times 10^3 \text{M}^{-1} \text{s}^{-1}$	35, 42

^aErrors are shown in parentheses. ^bMeasured by simulating the rate of generation and decay of the ascorbyl radical signal, followed by time-resolved EPR. ^cThe species in quotation marks is highly unstable, making the reaction as written very unfavorable. Species such as this will likely react very rapidly with other radicals, such as $\bullet\text{NO}$, or other sulfide-derived species, leading to polysulfides, and thus the species in quotation marks must be considered transient or a very short-lived intermediate. The second reaction could become thermodynamically favorable if another reactant X/X^{\bullet} reacts in a concerted or sequential fashion with a transient $\text{S}^{\bullet-}$ to produce a $\text{SY}^{\bullet-}$ or SY^- species. X/X^{\bullet} could be a sulfur-derived species, $\bullet\text{NO}$, or another sulfur-centered radical.

**Figure 2.** TPSSh-D3(BJ)/def2-TZVPP/CPCM(SMD)-optimized geometries for the first step proposed.

coupled reactions, which lead to more stable products and thus drive the reactions forward. However, the observed HNO production is compatible with a first-order rate on both $\bullet\text{NO}$ and RXH, and therefore we write these reactions in the simplest possible way, which does not capture the complete mechanism, only the dependence of HNO production on the reactant concentrations.

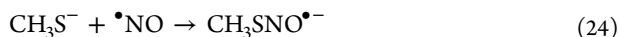
For the ascorbic acid and H_2S experiments, the traces could be simulated by considering only the formation and decay of the adduct, without the inclusion of a direct reaction ($k_{\text{H}_2\text{S,NO}}$ and $k_{\text{Asc,NO,direct}}$ were both set to $0 \text{M}^{-1} \text{s}^{-1}$). As can be seen from Figure 1 (left and right), the adduct model reproduces quite well the experimental traces. The adduct formation rates were $28 \text{M}^{-1} \text{s}^{-1}$ for the reaction between $\bullet\text{NO}$ and AAH^- and $8 \times 10^3 \text{M}^{-1} \text{s}^{-1}$ for the reaction between H_2S and $\bullet\text{NO}$. In the case of CysH, both pathways were considered, obtaining $180 \text{M}^{-1} \text{s}^{-1}$ for the direct route and $700\text{--}900 \text{M}^{-1} \text{s}^{-1}$ for the adduct formation route. The rate constants for AAH^- and CysH are already quite a bit larger than the previously determined “effective” rate constants. However, the direct rate constant for the reaction between NO and AAH^- , $k_{\text{Asc,NO,direct}}$

$= 43(15) \text{M}^{-1} \text{s}^{-1}$, measured by following the generation and decay of the ascorbyl radical signal by EPR,³⁶ is in good agreement with the value obtained in this work. Inclusion of the adduct formation reactions made it necessary to include the direct reaction of the adducts with the electrode, with forward and reverse rate constants provided in Table S1. It is important to note that the information derived from the electrochemical measurements does not allow one to determine the actual identity of the RX(HNO)^{\bullet} adducts, and especially the exact mechanism for its decomposition. The $k_{\text{RX(HNO),decay}}$ rate constants were obtained from the choice of a unimolecular decay route for the adducts, which was the simplest possible model. In the case of the ascorbic acid-derived adduct with HNO, a unimolecular decay route is likely, based on the experimental and mechanistic results previously reported.³⁶

On the other hand, it is clear that the reaction does not involve a simple outer-sphere reduction coupled to proton release/uptake, which is thermodynamically unfavorable as evidenced by the reduction potentials. $E'(\text{NO,H}^+/\text{HNO})$, at micromolar and picomolar concentrations of $\bullet\text{NO}$ and HNO,

respectively, is between -0.3 and 0 V at pH 7.4, and $E^{\circ}(\text{RO}^{\bullet},\text{H}^+/\text{ROH})$ for alcohols is between 0.10 and 0.97 V at pH 7.³⁶ In the case of the CysH- and H_2S -derived adducts with HNO, HNO release may result from a more complex mechanism. In the following sections, we show through AIMD and DFT calculations that the formation of an $\text{RSNO}^{\bullet-}$ adduct, as well as the $\text{RSN}(\text{O})\text{NO}^-$ adduct, is thermodynamically favored. $E^{\circ}(\text{RSSR},2\text{H}^+/2\text{RSH})$ is close to -0.25 V, and thus an outer-sphere electron transfer is, in principle, thermodynamically favorable.

3.2. Mechanism for the Reaction of 2 equiv of $\bullet\text{NO}$ with RS^- Species. We propose a two-step mechanism for reaction of the RS^- species with two $\bullet\text{NO}$ molecules,^{55–57} sequentially, as follows:



The optimized geometries were characterized as a local minimum by the absence of imaginary frequencies, while transition states were confirmed by the presence of a single imaginary frequency. Figure 2 shows the geometries for the first step of the sequential reaction of RS^- with two $\bullet\text{NO}$ molecules. In the figure, “Reac” stands for the isolated CH_3S^- and $\bullet\text{NO}$ molecules, “Int” represents the prereactive complex, “TS” corresponds to the transition state, and “Prod” stands for the product of the reaction. Figure 3 shows the Gibbs free energy profile for the reactants, precomplex, transition state, and product.

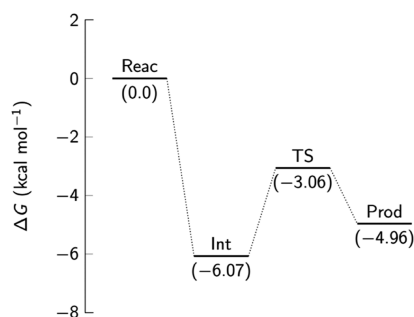


Figure 3. Reaction Gibbs free energy, in kcal mol^{-1} , for the first step of the proposed mechanism. The imaginary frequency for the transition state was evaluated as -85.42 cm^{-1} .

It is possible to observe that the prereactive complex significantly stabilizes the system by approximately 6 kcal mol^{-1} . From this stabilization, a low barrier of 3 kcal mol^{-1} is required for the formation of $\text{CH}_3\text{SNO}^{\bullet-}$. This product, as well as the product from the next step, involving the reaction with another $\bullet\text{NO}$ molecule, is in agreement with the formation of an adduct, as suggested by the kinetic data of structurally related thiols such as cysteine. Despite the fact of the intermediates being more stable than the product, this ΔG is not large and may be interpreted as the prereactive complex, with the product being in an equilibrium slightly shifted to the prereactive side. Another remark should be added regarding the N–O distance; Figure 2 shows that the formation of an intermediate and the following structures leads to a slight increase of the bond distance from 1.149 to 1.235 Å. This increase may be due to repulsion between the negative charge from CH_3S^- and the unpaired electron of $\bullet\text{NO}$.

Figures 4 and 5 show the optimized geometries and the ΔG profile for the second step of the proposed sequential

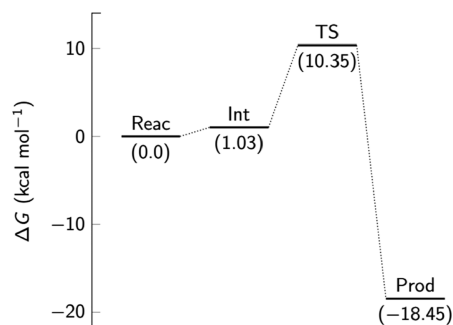


Figure 5. Reaction Gibbs free energy, in kcal mol^{-1} , for the second step in the proposed mechanism. The imaginary frequency for the transition state was evaluated as -552.71 cm^{-1} .

mechanism. It is possible to observe that the interaction between the reactants yields a species in which the nitric oxide molecules are in trans-like orientation. This structure is about 1 kcal mol^{-1} less stable than the reactants and transition state, which involves rotation of the NO moieties to reach a cis-like orientation. Despite the relatively high barrier, the energy cost for this rotational rearrangement is compensated for by the approximate 20 kcal mol^{-1} stabilization provided to the system.

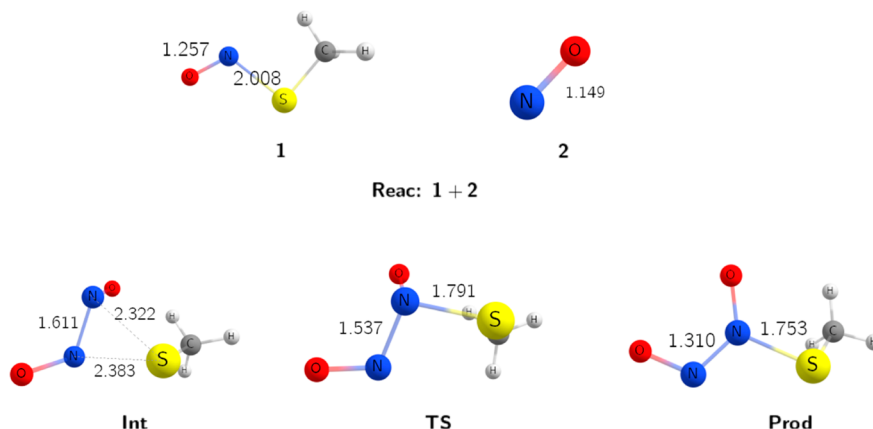


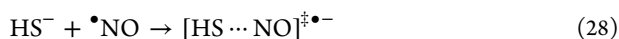
Figure 4. Optimized geometries for the second step in the proposed mechanism.

It is important to point out that the results shown above indicate that the second step of the proposed mechanism leads to a RSN(O)NO^- species in which the N–N bond is 1.6 Å. This value is significantly smaller than the N–N distance in the NO dimer of 2.1 Å obtained from the gas-phase MP2/def2-QZVP reference geometry. This effect probably occurs because of donation of the RS^- electron density to the ON–NO moiety of the products. Table S2 shows the CHELPG-calculated charges for the Int, TS, and Prod species. It is possible to observe that nitrogen atoms in the products have charges of opposite sign ($q_{\text{N-S-bonded}} = 0.837$ and $q_{\text{N-N-bonded}} = -0.397$), leading to an attractive electrostatic interaction and, consequently, the reduction of the N–N bond length.

3.4. Mechanism for the Reaction of 2 equiv of $\bullet\text{NO}$ with HS^- Species. In order to evaluate the Gibbs free energies and propose a molecular mechanism for the two-step reaction of $\bullet\text{NO}$ with HS^- , described by the chemical equations



we performed DFT calculations at the same level of theory of the above-shown RS^- species to find the reactants (Reac), intermediates (Int), transition states (TS), and products (Prod). After several unsuccessful attempts to obtain the TS for



we decided to perform a systematic procedure to obtain a reliable guess structure for this activated complex. We performed a set of 20 TPSSh-D3(BJ)def2-TZVPP/CPCM(SMD) geometry optimizations by varying the N–S distance from 3.2 to 1.2 Å. This potential energy surface (PES) corresponds to the reaction coordinate for the $\text{HS}^-/\text{H}_2\text{S}$ reaction with $\bullet\text{NO}$, as shown in Scheme 2.

Scheme 2. Representation of the Reaction Coordinate for Construction of the PES for $\text{HS}^- + \bullet\text{NO} \rightarrow \text{HSNO}^{\bullet-}$ (the Procedure for H_2S Was Similar)

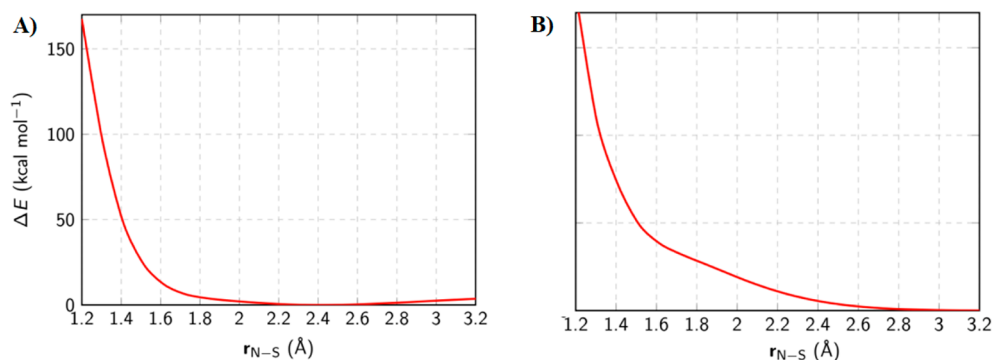
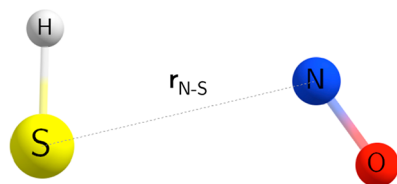


Figure 6. TPSSh-D3(BJ)/def2/TZVP/CPCM(SMD) PES surface as a function of the $r_{\text{N-S}}$ distance for $\bullet\text{NO}$ and (A) HS^- or (B) H_2S .

Figure 6 shows the PES as a function of the $r_{\text{N-S}}$ distance for the approach of the HS^- (A) and H_2S (B) species, respectively, to a $\bullet\text{NO}$ molecule. From these two figures, it is possible to observe that the interaction between these species is predominantly repulsive, reaching more than 150 kcal mol $^{-1}$ at 1.2 Å.

These results reveal that the two-step $\bullet\text{NO}$ consecutive reaction with $\text{H}_2\text{S}/\text{HS}^-$ may lead to high activation energies in the first step, and at this moment, we cannot provide a suitable reaction mechanism. Similar to the investigation on the reactivity of $(\text{NO})_2$ and RS^- species, we studied the reaction of the NO dimer with HS^- through the following reaction:



Figure 7 shows the optimized geometries of the reactants, intermediate, transition state, and products for the reaction of the NO dimer with HS^- . It can be seen that the N–N distance on $(\text{NO})_2$ is reduced by the formation of an entrance complex. After the formation of this intermediate, HS^- donates a proton to one $\bullet\text{NO}$, yielding HNO and a negatively charged SNO^- species.

Figure 8 shows the Gibbs free energy for the reaction coordinate. It is possible to observe that formation of the entrance complex, which shortens the N–N distance, stabilizes the reactants by approximately 6 kcal mol $^{-1}$. Once stabilized, a significant activation energy needs to be achieved in order to form the products. We speculate that, despite the low equilibrium constant for nitric oxide dimerization in the gas phase,^{58–63} this stable intermediate might be acting as the $(\text{NO})_2$ source because of the “accumulation” of this stable species. On the other hand, it is also possible that the reactants may not form the entrance complex, following a direct $\text{Reac} \rightarrow \text{TS}$ path in order to find an effective activation barrier of 12.26 kcal mol $^{-1}$ and yield the products, 3.46 kcal mol $^{-1}$ more stable than the reactants.

A summary of the energetics for the formation of several nitrosylated thiol species, as well as other products of the reactions of $\bullet\text{NO}$ with $\text{H}_2\text{S}/\text{HS}^-$ or CH_3S , is shown in Table 3, together with previously reported energetics for the formation of $\text{AAH}(\text{HNO})^{\bullet-}$, PhSNHO^\bullet , and $\text{CH}_3\text{SNHO}^\bullet$. The previously reported calculations were performed at levels of theory different from that used in this work. However, qualitative comparisons can be made for certain steps. For example, the activation energy for the reaction of $\bullet\text{NO}$ with CH_3SH is much larger than that for the reaction with CH_3S^- , and the latter reaction is also more favorable. This difference likely arises from the concerted proton rearrangement

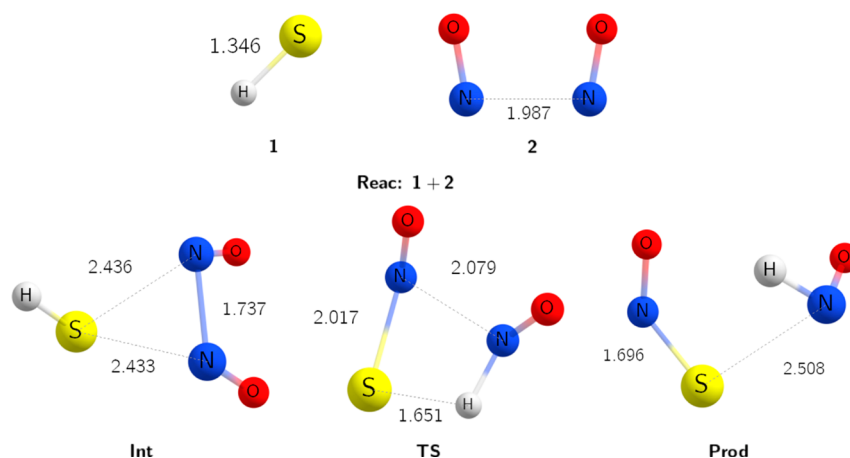


Figure 7. TPSSh-D3(BJ)/def2-TZVPP/CPSM(SMD)-optimized geometries for the direct reaction of HS⁻ with the NO dimer.

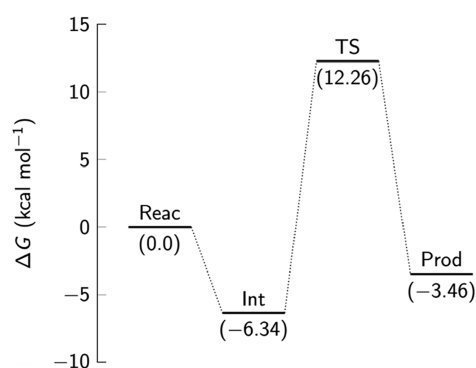


Figure 8. TPSSh-D3(BJ)/def2-TZVPP/CPCM(SMD) Gibbs free energy, in kcal mol⁻¹, for the reaction of HS⁻ with (NO)₂. The imaginary frequency for the transition state was evaluated as -1179.24 cm⁻¹.

occurring in the reaction of [•]NO with CH₃SH. A similarly large activation energy was found for the reaction of PhSH with [•]NO. The reaction of AAH⁻ with [•]NO was found to produce an AA(HNO)^{•-} intermediate (ascorbic acid has two vicinal acidic hydrogen atoms). This intermediate (detected by MS)³⁶ was calculated to be +16 kcal mol⁻¹ above the reactants, but the reaction was found to move forward by a series of exergonic steps, such as HNO dissociation to produce AA^{•-}

(detected by EPR). Because HNO rapidly reacts with [•]NO or HNO and the ascorbyl radical disproportionates (less rapidly) to ascorbate and dehydroascorbate, the relatively high energy of the intermediate is compensated for.

From the entries in Table 3, we can observe some striking tendencies regarding the reactivity of RSH with [•]NO. The reaction seems to become less favorable in the order R = Me, Ph, and H, with the reaction between H₂S and [•]NO being extremely unfavorable. The pK_a of PhSH is 6.62, while that of CH₃SH is 10.4, and that of H₂S is 6.90.⁶⁴ There does not seem to be a correlation between the activation energies and pK_a of the thiols. A similar tendency can be observed when CH₃S⁻ and HS⁻ reactivity is compared with that of [•]NO. In these cases, acidity is not a factor, so perhaps the dominating factor is the stabilization of the sulfur-centered radical during the reaction. In this regard, methyl or phenyl substituents could play a role in the stabilization of a radical compared to H. However, experimentally, the reaction between [•]NO and H₂S/HS⁻ shows the fastest reaction constant, followed by PhSH and cysteine (which could be considered the most similar to CH₃SH).³⁷ This trend is the inverse of that predicted by the calculations of the transition states obtained by the reaction of these sulfur compounds with [•]NO. It is observed that the activation energies for direct H₂S/HS⁻ with [•]NO are much higher compared to those of RSH (R = CH₃, Ph). Therefore, a

Table 3. Summary of Energetics (Gibbs Free Energies) Obtained for the Reactions of Thiols/Thiolates with [•]NO and (NO)₂ and Previously Reported Reactions of Ascorbyl Anion and Thiophenol with NO^a

	Int (kcal mol ⁻¹)	TS (kcal mol ⁻¹)	ΔG [‡] (kcal mol ⁻¹)	Prod (kcal mol ⁻¹)	ref
AAH ⁻ + [•] NO → AA(HNO) ^{•-}		n.d.	n.d.	+16	<i>b</i> , 36
PhSH + [•] NO → PhSNHO [•]	0	19.67	19.67	-2.51	<i>c</i> , 37
CH ₃ SH + [•] NO → CH ₃ SNHO [•]	0	23.36	23.36	-0.68	<i>c</i> , 37
CH ₃ S ⁻ + [•] NO → CH ₃ SNO ^{•-}	-6.07	-3.06	3.01	-4.96	<i>d</i>
CH ₃ SNO ^{•-} + [•] NO → CH ₃ SN(O)NO ⁻	1.03	10.35	9.32	-18.45	<i>d</i>
CH ₃ SN(H)O [•] + [•] NO → CH ₃ SN(O)NOH		n.d.	n.d.	-11.46	<i>d</i>
CH ₃ SN(O)NOH → CH ₃ SN(O)N(H)O		n.d.	n.d.	9.69	<i>d</i>
CH ₃ SN(O)N(H)O → CH ₃ SNO + HNO		n.d.	n.d.	4.18	<i>d</i>
HS ⁻ + [•] NO → SNOH ^{•-}	55.07	85.18	30.11	63.48	<i>d</i>
H ₂ S + [•] NO → [HSNHO] [•]	4.86	40.99	36.13	19.23	<i>d</i>
HS ⁻ + (NO) ₂ → SNO ⁻ + HNO	-6.34	12.26	18.6	-3.46	<i>d</i>

^aΔG[‡] = G(TS) - G(Int). ^bCalculated at the B3LYP/6-31G(d,p)/CPCM level. ^cCalculated at the TPSSh/def2-TZVP/CPCM(SMD) level plus two explicit water molecules. ^dCalculated at the TPSSh-D3(BJ)/def2-TZVPP/CPCM(SMD) level of theory. The geometries and ΔG profiles are shown in Figures S8–S15.

more complicated mechanism than a simple bimolecular reaction between $\bullet\text{NO}$ and $\text{H}_2\text{S}/\text{HS}^-$ seems to be taking place. Figures S10–S15 show that, in contrast to the reaction mechanism for methyl and phenyl groups, the reactions of $\bullet\text{NO}$ with $\text{H}_2\text{S}/\text{HS}^-$, in principle, do not occur through N–S bonding but by proton transfer, which leads to N–S coordination. It is also important to highlight that the energy barriers for the formation of intermediates and transition states, despite being higher than those for RSH, are lower for H_2S in comparison to HS^- by approximately 40 kcal mol^{-1} . On the other hand, the reaction of HS^- with $(\text{NO})_2$ is quite favorable and could be taking place. Previously carried out experiments show that this reaction is not first-order in NO under all experimental conditions but shows from a kinetic standpoint an intermediate order between 1 and 2, particularly at higher concentrations of NO. This will be further investigated from theoretical and experimental points of view and informed in a near future.

The experimental bimolecular rate constants between RXH and $\bullet\text{NO}$ allowed us to calculate the activation free energies ΔG^\ddagger , using the Eyring equation, as described in the SI. The equilibrium constant K_{eq} for formation of the reactant complex from the individual reactants, was assumed to be equal to 1 M^{-1} because this value was not available for AAH $^-$ or CysH, and for H_2S or HS^- , the energies of formation of the intermediate differ considerably. The obtained activation free energies were $15.6 \text{ kcal mol}^{-1}$ (AAH $^-$), $14.5 \text{ kcal mol}^{-1}$ (CysH), and $12.2 \text{ kcal mol}^{-1}$ (HS^-). These values show a relatively low dispersion, but because the K_{eq} values likely differ between reactions and from the value of 1 M^{-1} , we cannot at this point directly compare the activation energies derived from the experimental bimolecular constants and theoretical values.

Finally, the previous calculations show that the $\text{RSNO}^{\bullet-}$ (R = Ph, Me) and $\text{RSN}(\text{O})\text{NO}^-$ or $\text{SN}(\text{O})\text{NO}^{2-}$ adducts are clearly stable with respect to the reactants, supporting inclusion of the adduct hypothesis in the electrochemical kinetic modeling. There are various ways in which these adducts can decay and release HNO. $\text{RSNO}^{\bullet-}$ can be protonated to give HNO and RS^\bullet , which would rapidly dimerize or react further. As a representative example, we have calculated one possible pathway by which $\text{RSN}(\text{O})\text{NOH}$ can also release HNO and RSNO through a series of intramolecular proton-transfer reactions, as shown in Table 3 for R = Me. At this point, we have only calculated the free energies of reaction for each of these steps. The first steps, leading from CH_3SH to $\text{CH}_3\text{SN}(\text{O})\text{NOH}$ through a sequential reaction with two $\bullet\text{NO}$ molecules, are exergonic, while the following steps, leading to CH_3SNO and HNO, are slightly endergonic. This is entirely compatible with the experimentally inferred formation of an adduct between RXH and $\bullet\text{NO}$, followed by a slow release of HNO. In the context of the electrochemical measurements, both adducts could react with cobalt(III) porphyrin, directly generating $\text{Co}^{\text{III}}(\text{Por})(\text{NO}^-)$ and RS^\bullet or RSNO .

4. CONCLUSIONS

It is noted that $\bullet\text{NO}$ and HNO can be interconverted in biologically compatible media, depending on the redox state of the environment. We have shown that the direct reaction rate constants between NO and moderate reducing agents producing HNO are up to 30 times higher than the previously

reported k_{eff} values. These new higher values extend the idea that reducing or hypoxic environments are expected to generate HNO from nitric oxide. Nitroxyl is becoming acknowledged as an endogenously produced messenger that mediates specific physiological responses, many of which were attributed yet to direct $\bullet\text{NO}$ effects. For example, it is known that H_2S may transform endogenous NO^\bullet to HNO, which in cells activates the HNO/transient receptor potential channel/calcitonin gene-related peptide cascade, via the formation of disulfide bonds, which results in continuous calcium influx. This cascade regulates blood pressure and control of cardiac contractility (unlike NO^\bullet), suggesting broad physiological relevance of the findings. We have shown that the rate of HNO production through an anaerobic reaction between NO^\bullet and $\text{H}_2\text{S}/\text{HS}^-$ is orders of magnitude faster than that for any known HNO donor and could be taking place because of the stabilization of $(\text{NO})_2$ by the negatively charged HS^- . The intermediate shown in Figure 7 has an N–N bond distance that is 0.25 \AA shorter than that in free $(\text{NO})_2$. On the other hand, we also showed that the reaction of the successive attack by two NO molecules to biologically compatible compounds could produce HNO. The results summarized in Table 3 suggest deprotonated adducts of the type $\text{RXNO}^{\bullet-}$ to be more stable and to require lower activation energies to form compared to protonated adducts of the type $\text{RX}(\text{HNO})^\bullet$, with the exception being R = H. Therefore, detailed mechanistic reinvestigations of the reactions of NO with aromatic alcohols are warranted.

■ ASSOCIATED CONTENT

Supporting Information

The Supporting Information is available free of charge at <https://pubs.acs.org/doi/10.1021/acs.inorgchem.1c01061>.

Description of the procedures for kinetic simulations, set of differential equations that describe the reactions occurring at the surface of the electrode, electronic structure calculation details, as-optimized geometries, Gibbs free energy, and CHELPG charges calculated for intermediates, transition states, and products (PDF)

■ AUTHOR INFORMATION

Corresponding Authors

Sebastián A. Suárez – *Departamento de Química Inorgánica, Analítica y Química Física, Facultad de Ciencias Exactas y Naturales, Universidad de Buenos Aires, Buenos Aires C1053, Argentina; INQUIMAE-CONICET, Ciudad Universitaria, Buenos Aires C1428EHA, Argentina; orcid.org/0000-0003-0236-5743; Email: seba@qi.fcen.uba.ar*

Fabio Doctorovich – *Departamento de Química Inorgánica, Analítica y Química Física, Facultad de Ciencias Exactas y Naturales, Universidad de Buenos Aires, Buenos Aires C1053, Argentina; INQUIMAE-CONICET, Ciudad Universitaria, Buenos Aires C1428EHA, Argentina; orcid.org/0000-0003-1088-2089; Email: doctorovich@qi.fcen.uba.ar*

Authors

Nicolas I. Neuman – *Instituto de Desarrollo Tecnológico para la Industria Química, INTEC, UNL-CONICET, Paraje El Pozo, Santa Fe 3000, Argentina; Institut für Anorganische Chemie, Universität Stuttgart, Stuttgart D-70569, Germany; orcid.org/0000-0003-3368-0228*

Mateus F. Venâncio – Departamento de Físico-Química, Instituto de Química, Universidade Federal da Bahia, Salvador, Bahia 40170-110, Brazil

William R. Rocha – Departamento de Química, Instituto de Ciências Exatas, Universidade Federal de Minas Gerais, Belo Horizonte, Minas Gerais 31270-901, Brazil; orcid.org/0000-0002-0025-2158

Damian E. Bikiel – Departamento de Química Inorgánica, Analítica y Química Física, Facultad de Ciencias Exactas y Naturales, Universidad de Buenos Aires, Buenos Aires C1053, Argentina; INQUIMAE-CONICET, Ciudad Universitaria, Buenos Aires C1428EHA, Argentina

Complete contact information is available at:

<https://pubs.acs.org/10.1021/acs.inorgchem.1c01061>

Author Contributions

[†]These authors contributed equally. The manuscript was written through contributions of all authors. All authors have given approval to the final version of the manuscript.

Notes

The authors declare no competing financial interest.

ACKNOWLEDGMENTS

The research reported in this publication was supported by the Ministerio de Ciencia, Tecnología e Innovación Productiva (Grants PICT-2015-3854 and PICT-2017-1930) and the Universidad de Buenos Aires (UBACYT) Project 20020170100595SBA. N.I.N., D.E.B., S.A.S., and F.D. are members of CONICET. M.F.V. and W.R.R. thank the Conselho Nacional de Desenvolvimento Científico e Tecnológico, INCT-Catálise, and Fundação de Amparo à Pesquisa do Estado de Minas Gerais for financial support.

REFERENCES

- (1) McCleverty, J. A. Chemistry of Nitric Oxide Relevant to Biology. *Chem. Rev.* **2004**, *104* (2), 403–418.
- (2) Stamler, J. S.; Singel, D. J.; Loscalzo, J. Biochemistry of Nitric Oxide and Its Redox-Activated Forms. *Science (Washington, DC, U. S.)* **1992**, *258* (5090), 1898–1902.
- (3) Stuehr, D. J.; Haque, M. M. Nitric Oxide Synthase Enzymology in the 20 Years after the Nobel Prize. *Br. J. Pharmacol.* **2019**, *176* (2), 177–188.
- (4) Ignarro, L. J. Nitric Oxide Is Not Just Blowing in the Wind. *Br. J. Pharmacol.* **2019**, *176* (2), 131–134.
- (5) Cheng, J.; He, K.; Shen, Z.; Zhang, G.; Yu, Y.; Hu, J. Nitric Oxide (NO)-Releasing Macromolecules: Rational Design and Biomedical Applications. *Front. Chem.* **2019**, *7*. DOI: [10.3389/fchem.2019.00530](https://doi.org/10.3389/fchem.2019.00530).
- (6) Vanhoutte, P. M.; Zhao, Y.; Xu, A.; Leung, S. W. S. Thirty Years of Saying NO. *Circ. Res.* **2016**, *119* (2), 375–396.
- (7) Radi, R. Oxygen Radicals, Nitric Oxide, and Peroxynitrite: Redox Pathways in Molecular Medicine. *Proc. Natl. Acad. Sci. U. S. A.* **2018**, *115* (23), 5839–5848.
- (8) Lancaster, J. R. Historical Origins of the Discovery of Mammalian Nitric Oxide (Nitrogen Monoxide) Production/Physiology/Pathophysiology. *Biochem. Pharmacol.* **2020**, *176*, 113793.
- (9) Chiesa, J. J.; Baidanoff, F. M.; Golombek, D. A. Don't Just Say No: Differential Pathways and Pharmacological Responses to Diverse Nitric Oxide Donors. *Biochem. Pharmacol.* **2018**, *156*, 1–9.
- (10) Bruce King, S. Potential Biological Chemistry of Hydrogen Sulfide (H₂S) with the Nitrogen Oxides. *Free Radical Biol. Med.* **2013**, *55*, 1–7.
- (11) Irvine, J. C.; Ritchie, R. H.; Favaloro, J. L.; Andrews, K. L.; Widdop, R. E.; Kemp-Harper, B. K. Nitroxyl (HNO): The Cinderella of the Nitric Oxide Story. *Trends Pharmacol. Sci.* **2008**, *29* (12), 601–608.
- (12) Flores-Santana, W.; Salmon, D. J.; Donzelli, S.; Switzer, C. H.; Basudhar, D.; Ridnour, L.; Cheng, R.; Glynn, S. A.; Paolucci, N.; Fukuto, J. M.; Miranda, K. M.; Wink, D. A. The Specificity of Nitroxyl Chemistry Is Unique Among Nitrogen Oxides in Biological Systems. *Antioxid. Redox Signaling* **2011**, *14* (9), 1659–1674.
- (13) Miranda, K. The Chemistry of Nitroxyl (HNO) and Implications in Biology. *Coord. Chem. Rev.* **2005**, *249* (3–4), 433–455.
- (14) Shafirovich, V.; Lyman, S. V. Nitroxyl and Its Anion in Aqueous Solutions: Spin States, Protic Equilibria, and Reactivities toward Oxygen and Nitric Oxide. *Proc. Natl. Acad. Sci. U. S. A.* **2002**, *99* (11), 7340–7345.
- (15) Lyman, S. V.; Shafirovich, V.; Poskrebyshev, G. A. One-Electron Reduction of Aqueous Nitric Oxide: A Mechanistic Revision. *Inorg. Chem.* **2005**, *44* (15), 5212–5221.
- (16) Miranda, K. M.; Nims, R. W.; Thomas, D. D.; Espey, M. G.; Citrin, D.; Bartberger, M. D.; Paolucci, N.; Fukuto, J. M.; Feelisch, M.; Wink, D. A. Comparison of the Reactivity of Nitric Oxide and Nitroxyl with Heme Proteins: A Chemical Discussion of the Differential Biological Effects of These Redox Related Products of NOS. *J. Inorg. Biochem.* **2003**, *93* (1–2), 52–60.
- (17) Liochev, S. I.; Fridovich, I. The Mode of Decomposition of Angeli's Salt (Na₂N₂O₃) and the Effects Thereon of Oxygen, Nitrite, Superoxide Dismutase, and Glutathione. *Free Radical Biol. Med.* **2003**, *34* (11), 1399–1404.
- (18) Fukuto, J. M. A Recent History of Nitroxyl Chemistry, Pharmacology and Therapeutic Potential. *Br. J. Pharmacol.* **2019**, *176* (2), 135–146.
- (19) Doctorovich, F.; Farmer, P. J.; Marti, M. A. *The Chemistry and Biology of Nitroxyl (HNO)*; Elsevier, 2016; Vol. 53; DOI: [10.1016/c2013-0-18854-x](https://doi.org/10.1016/c2013-0-18854-x).
- (20) Van Stappen, C.; Goodrich, L. E.; Lehnert, N. The Interaction of HNO With Transition Metal Centers and Its Biological Significance. Insight Into Electronic Structure From Theoretical Calculations. *The Chemistry and Biology of Nitroxyl (HNO)*; Elsevier, 2017; pp 155–192; DOI: [10.1016/B978-0-12-800934-5.00008-6](https://doi.org/10.1016/B978-0-12-800934-5.00008-6).
- (21) Ford, P. C.; Lorkovic, I. M. Mechanistic Aspects of the Reactions of Nitric Oxide with Transition-Metal Complexes. *Chem. Rev.* **2002**, *102* (4), 993–1018.
- (22) Doctorovich, F.; Bikiel, D. E.; Pellegrino, J.; Suárez, S. A.; Marti, M. A. Azanone (HNO) Interaction with Hemeproteins and Metalloporphyrins. *Adv. Inorg. Chem.* **2012**, *64*, 97–139.
- (23) Khade, R. L.; Yang, Y.; Shi, Y.; Zhang, Y. HNO-Binding in Heme Proteins: Effects of Iron Oxidation State, Axial Ligand, and Protein Environment. *Angew. Chem.* **2016**, *128* (48), 15282–15285.
- (24) Globins and Other Nitric Oxide-Reactive Proteins. *Methods in Enzymology*; Elsevier, 2008; Vol. 436, Part A; DOI: [10.1016/S0076-6879\(08\)X3601-8](https://doi.org/10.1016/S0076-6879(08)X3601-8).
- (25) Miranda, K. M.; Nims, R. W.; Thomas, D. D.; Espey, M. G.; Citrin, D.; Bartberger, M. D.; Paolucci, N.; Fukuto, J. M.; Feelisch, M.; Wink, D. A. Comparison of the Reactivity of Nitric Oxide and Nitroxyl with Heme Proteins. *J. Inorg. Biochem.* **2003**, *93* (1–2), 52–60.
- (26) Paolucci, N.; Jackson, M. I.; Lopez, B. E.; Miranda, K.; Tocchetti, C. G.; Wink, D. A.; Hobbs, A. J.; Fukuto, J. M. The Pharmacology of Nitroxyl (HNO) and Its Therapeutic Potential: Not Just the Janus Face of NO. *Pharmacol. Ther.* **2007**, *113* (2), 442–458.
- (27) Fukuto, J. M.; Cisneros, C. J.; Kinkade, R. L. A Comparison of the Chemistry Associated with the Biological Signaling and Actions of Nitroxyl (HNO) and Nitric Oxide (NO). *J. Inorg. Biochem.* **2013**, *118*, 201–208.
- (28) Bartberger, M. D.; Liu, W.; Ford, E.; Miranda, K. M.; Switzer, C.; Fukuto, J. M.; Farmer, P. J.; Wink, D. A.; Houk, K. N. The Reduction Potential of Nitric Oxide (NO) and Its Importance to NO Biochemistry. *Proc. Natl. Acad. Sci. U. S. A.* **2002**, *99* (17), 10958–10963.

- (29) Venâncio, M. F.; Doctorovich, F.; Rocha, W. R. Solvation and Proton-Coupled Electron Transfer Reduction Potential of 2 NO • to 1 HNO in Aqueous Solution: A Theoretical Investigation. *J. Phys. Chem. B* **2017**, *121* (27), 6618–6625.
- (30) Ehman, D. L.; Sawyer, D. T. Electrochemistry of Nitric Oxide and of Nitrous Acid at a Mercury Electrode. *J. Electroanal. Chem. Interfacial Electrochem.* **1968**, *16* (4), 541–549.
- (31) Benderskii, V. A.; Krivenko, A. G.; P, E. A. Homogenous and Electrode Reactions of NO₂²⁻ Ions. *Sov. Electrochem. Engl. Tr.* **1989**, *25*, 154–161.
- (32) Anderson, W. R. Heats of formation of HNO and some related species. *Combust. Flame* **1999**, *117*, 394–403.
- (33) Pryor, W. A.; Church, D. F.; Govindan, C. K.; Crank, G. Oxidation of Thiols by Nitric Oxide and Nitrogen Dioxide: Synthetic Utility and Toxicological Implications. *J. Org. Chem.* **1982**, *47* (1), 156–159.
- (34) DeMaster, E. G.; Quast, B. J.; Redfern, B.; Nagasawa, H. T. Reaction of Nitric Oxide with the Free Sulfhydryl Group of Human Serum Albumin Yields a Sulfenic Acid and Nitrous Oxide. *Biochemistry* **1995**, *34* (36), 11494–11499.
- (35) Eberhardt, M.; Dux, M.; Namer, B.; Miljkovic, J.; Cordasic, N.; Will, C.; Kichko, T. I.; de la Roche, J.; Fischer, M.; Suárez, S. A.; Bikiel, D.; Dorsch, K.; Leffler, A.; Babes, A.; Lampert, A.; Lennerz, J. K.; Jacobi, J.; Martí, M. A.; Doctorovich, F.; Högestätt, E. D.; Zygumt, P. M.; Ivanovic-Burmazovic, I.; Messlinger, K.; Reeh, P.; Filipovic, M. R. H₂S and NO Cooperatively Regulate Vascular Tone by Activating a Neuroendocrine HNO–TRPA1–CGRP Signalling Pathway. *Nat. Commun.* **2014**, *5* (1), 4381.
- (36) Suarez, S. A.; Neuman, N. I.; Muñoz, M.; Álvarez, L.; Bikiel, D. E.; Brondino, C. D.; Ivanović-Burmazović, I.; Miljkovic, J. L.; Filipovic, M. R.; Martí, M. A.; Doctorovich, F. Nitric Oxide Is Reduced to HNO by Proton-Coupled Nucleophilic Attack by Ascorbate, Tyrosine, and Other Alcohols. A New Route to HNO in Biological Media? *J. Am. Chem. Soc.* **2015**, *137* (14), 4720–4727.
- (37) Suarez, S. A.; Muñoz, M.; Alvarez, L.; Venâncio, M. F.; Rocha, W. R.; Bikiel, D. E.; Martí, M. A.; Doctorovich, F. HNO Is Produced by the Reaction of NO with Thiols. *J. Am. Chem. Soc.* **2017**, *139* (41), 14483–14487.
- (38) Hamer, M.; Suarez, S. A.; Muñoz, M.; Álvarez, L.; Martí, M.; Doctorovich, F. Reaction of Amines with NO at Room Temperature and Atmospheric Pressure: Is Nitroxyl a Reaction Intermediate? *Pure Appl. Chem.* **2020**, *92* (12), 2005–2014.
- (39) Hamer, M.; Suarez, S. A.; Neuman, N. I.; Alvarez, L.; Muñoz, M.; Martí, M. A.; Doctorovich, F. Discussing Endogenous NO • /HNO Interconversion Aided by Phenolic Drugs and Vitamins. *Inorg. Chem.* **2015**, *54* (19), 9342–9350.
- (40) Marcolongo, J. P.; Venâncio, M. F.; Rocha, W. R.; Doctorovich, F.; Olabe, J. A. NO/H₂S “Crosstalk” Reactions. The Role of Thionitrites (SNO –) and Perthionitrites (SSNO –). *Inorg. Chem.* **2019**, *58* (22), 14981–14997.
- (41) Filipovic, M. R.; Eberhardt, M.; Prokopovic, V.; Mijuskovic, A.; Orescanin-Dusic, Z.; Reeh, P.; Ivanovic-Burmazovic, I. Beyond H₂S and NO Interplay: Hydrogen Sulfide and Nitroprusside React Directly to Give Nitroxyl (HNO). A New Pharmacological Source of HNO. *J. Med. Chem.* **2013**, *56* (4), 1499–1508.
- (42) Suarez, S. A.; Vargas, P.; Doctorovich, F. A. Updating NO•/HNO Interconversion under Physiological Conditions: A Biological Implication Overview. *J. Inorg. Biochem.* **2021**, *216*, 111333.
- (43) Suárez, S. A.; Fonticelli, M. H.; Rubert, A. A.; de la Llave, E.; Scherlis, D. D.; Salvarezza, R. C.; Martí, M. A.; Doctorovich, F. A Surface Effect Allows HNO/NO Discrimination by a Cobalt Porphyrin Bound to Gold. *Inorg. Chem.* **2010**, *49* (15), 6955–6966.
- (44) Suárez, S. A.; Bikiel, D. E.; Wetzler, D. E.; Martí, M. A.; Doctorovich, F. Time-Resolved Electrochemical Quantification of Azanone (HNO) at Low Nanomolar Level. *Anal. Chem.* **2013**, *85* (21), 10262–10269.
- (45) Doctorovich, F.; Suárez, S. A.; Martí, M. A.; Battaglini, F. HNO Biosensor. International Patent WO2020/136414A1, 2018.
- (46) Heinecke, J. L.; Khin, C.; Pereira, J. C. M.; Suárez, S. A.; Iretskii, A. V.; Doctorovich, F.; Ford, P. C. Nitrite Reduction Mediated by Heme Models. Routes to NO and HNO? *J. Am. Chem. Soc.* **2013**, *135* (10), 4007–4017.
- (47) Eaton, J. W.; Bateman, D.; Hauberg, S.; Wehbring, R. GNU Octave Version 6.1.0 Manual: A High-Level Interactive Language for Numerical Computations; 2020; <https://www.gnu.org/software/octave/doc/v6.1.0/>.
- (48) Miranda, K. M.; Dutton, A. S.; Ridnour, L. A.; Foreman, C. A.; Ford, E.; Paolucci, N.; Katori, T.; Tocchetti, C. G.; Mancardi, D.; Thomas, D. D.; Espey, M. G.; Houk, K. N.; Fukuto, J. M.; Wink, D. A. Mechanism of Aerobic Decomposition of Angeli’s Salt (Sodium Trioxodinitrate) at Physiological PH. *J. Am. Chem. Soc.* **2005**, *127* (2), 722–731.
- (49) Weigend, F.; Ahlrichs, R. Balanced Basis Sets of Split Valence, Triple Zeta Valence and Quadruple Zeta Valence Quality for H to Rn: Design and Assessment of Accuracy. *Phys. Chem. Chem. Phys.* **2005**, *7* (18), 3297.
- (50) Tao, J.; Perdew, J. P.; Staroverov, V. N.; Scuseria, G. E. Climbing the Density Functional Ladder: Nonempirical Meta-Generalized Gradient Approximation Designed for Molecules and Solids. *Phys. Rev. Lett.* **2003**, *91* (14), 146401.
- (51) Staroverov, V. N.; Scuseria, G. E.; Tao, J.; Perdew, J. P. Erratum: “Comparative Assessment of a New Nonempirical Density Functional: Molecules and Hydrogen-Bonded Complexes” [J. Chem. Phys. **119**, 12129 (2003)]. *J. Chem. Phys.* **2004**, *121* (22), 11507.
- (52) Barone, V.; Cossi, M. Quantum Calculation of Molecular Energies and Energy Gradients in Solution by a Conductor Solvent Model. *J. Phys. Chem. A* **1998**, *102* (11), 1995–2001.
- (53) Marenich, A. V.; Cramer, C. J.; Truhlar, D. G. Universal Solvation Model Based on Solute Electron Density and on a Continuum Model of the Solvent Defined by the Bulk Dielectric Constant and Atomic Surface Tensions. *J. Phys. Chem. B* **2009**, *113* (18), 6378–6396.
- (54) Neese, F. Software Update: The ORCA Program System, Version 4.0. *Wiley Interdiscip. Rev.: Comput. Mol. Sci.* **2018**, *8* (1). DOI: 10.1002/wcms.1327.
- (55) Littlejohn, D.; Hu, K. Y.; Chang, S. G. Kinetics of the Reaction of Nitric Oxide with Sulfite and Bisulfite Ions in Aqueous Solution. *Inorg. Chem.* **1986**, *25* (18), 3131–3135.
- (56) Grossi, L. Nitric Oxide: Probably the in Vivo Mediator of the Bisulfite’s Effects. *J. Biosci. Med.* **2014**, *02* (07), 1–6.
- (57) Lepentiotis, V.; Prinsloo, F. F.; van Eldik, R.; Gutberlet, H. Influence of Mixed Sulfur–Nitrogen Oxides on the Redox Kinetics of Iron Ions in Aqueous Solution. *J. Chem. Soc., Dalton Trans.* **1996**, No. 10, 2135–2141.
- (58) Billingsley, J.; Callear, A. B. Investigation of the 2050 Å System of the Nitric Oxide Dimer. *Trans. Faraday Soc.* **1971**, *67*, 589–597.
- (59) Dinerman, C. E.; Ewing, G. E. Infrared Spectrum, Structure, and Heat of Formation of Gaseous (NO)₂. *J. Chem. Phys.* **1970**, *53* (2), 626–631.
- (60) Forte, E.; Van Den Bergh, H. The Heat of Formation of the Nitric Oxide Dimer and Its UV Spectrum. *Chem. Phys.* **1978**, *30* (3), 325–331.
- (61) Kukolich, S. G. Structure of the NO Dimer. *J. Am. Chem. Soc.* **1982**, *104* (17), 4715–4716.
- (62) Guggenheim, E. A.; Scott, R. L.; Guggenheim, E. A. Dimerization of Gaseous Nitric Oxide. *Mol. Phys.* **1966**, *10* (4), 401–404.
- (63) Smith, A. L.; Johnston, H. L. The Magnetic Susceptibility of Liquid Nitric Oxide and the Heat of Dissociation of (NO)₂. *J. Am. Chem. Soc.* **1952**, *74* (18), 4696–4698.
- (64) Serjeant, E. P.; Dempsey, B. *Ionisation Constants of Organic Acids in Aqueous Solution. International Union of Pure and Applied Chemistry (IUPAC); IUPAC Chemical Data Series No. 23; Pergamon Press, Inc.: New York, 1979; p 165.*